

## Article

# Study of the Stability of the Surface Perilous Rock in a Mining Area

Lu Gao <sup>†</sup>, Xiangtao Kang <sup>\*,†</sup>, Lin Gao <sup>†</sup> and Zhenqian Ma <sup>†</sup>

Mining College, Guizhou University, Guiyang 550025, China; lulu925518@163.com (L.G.); lgao@gzu.edu.cn (L.G.); zqma@gzu.edu.cn (Z.M.)

\* Correspondence: xiaokangedu@163.com

† These authors contributed equally to this work.

**Abstract:** As a result of the mining of a C3 coal seam in a mine in Guizhou, perilous rock masses on the surface collapsed. In this study, the stability of perilous rock masses on the surface of the coal mine before and after mining was calculated and examined, and the movement law of the overlying strata in the goaf, the movement and deformation law, and the failure mode of perilous rock were analyzed. This study provides a theoretical basis for the treatment of unstable rock and coal seam mining, and has important guiding significance for the safe and efficient production of the mine. The results show that: (1) The perilous rock is in a basically stable state without the influence of mining. Through theoretical analysis and the construction of the collapse model of perilous rock, it is judged that perilous rocks W1, W3, W4, and W7 were basically stable, perilous rocks W2 and W5 were in an unstable state, and perilous rock W6 was stable without heavy rainfall. (2) As a result of the mining of the C3 coal seam, the cracks in the upper strata began to develop to the surface, and the longitudinal separation cracks gradually appeared between the surface perilous rock and the rock matrix. Due to the existence of these cracks, the perilous rock had a downward shear force. In addition, due to the heavy rainfall in the Guizhou area, the transient saturated zone of perilous rock is expanding and the strength of perilous rock is reduced. The seepage increases the sliding force of the perilous rock and aggravates the opening of cracks at any time. (3) The stability of the surface perilous rock mass is largely affected by the mining of underground coal mines. The simulation analysis was repeated using the method of setting coal pillars. When 45 m permanent protection coal pillars are set at both ends, and 15 m local protection coal pillars are set at 60 m, the safety of coal mining can be ensured without affecting the surface and perilous rock.

**Keywords:** perilous rock stability; coal seam mining; UDEC; rockfall; safety production



**Citation:** Gao, L.; Kang, X.; Gao, L.; Ma, Z. Study of the Stability of the Surface Perilous Rock in a Mining Area. *Energies* **2022**, *15*, 1542.

<https://doi.org/10.3390/en15041542>

Academic Editors: Junlong Shang, Chun Zhu, Manchao He and Manoj Khandelwal

Received: 12 January 2022

Accepted: 16 February 2022

Published: 19 February 2022

**Publisher's Note:** MDPI stays neutral with regard to jurisdictional claims in published maps and institutional affiliations.



**Copyright:** © 2022 by the authors. Licensee MDPI, Basel, Switzerland. This article is an open access article distributed under the terms and conditions of the Creative Commons Attribution (CC BY) license (<https://creativecommons.org/licenses/by/4.0/>).

## 1. Introduction

The surface perilous rock mass in a mining area refers to the rock structure that is distributed on a steep slope or cliff at the surface of the mine. Under the action of external forces, such as natural conditions or mining engineering activities, perilous rock is in, or near, the limit of the equilibrium state in which cracks or structural planes develop [1–5]. As a result of the rapid development of China's construction sector, human engineering activities have increased rapidly in many southwest regions of China's mountains, and perilous rock collapse disasters often occur [6–8]. Guizhou Province, China, is characterized by special karst landforms, and its geological and topographical conditions are relatively complex. Thus, coal mining can easily cause accidents involving the collapse of surface perilous rock [9–12]. Therefore, the exploration of the stability of overlying strata in the goaf is a well-studied and difficult scientific and engineering technology problem in the global field of engineering geology.

Qian et al. [13] proposed the key stratum theory of strata movement and control in 1996, which challenged the limitations of traditional mining surface movement and

deformation research, and opened up a new perspective for ground surface subsidence research. Xu et al. [14] studied the dynamic process of the key strata of the overlying strata on the surface subsidence. Baryarkh et al. [15] established a dynamic surface subsidence prediction method with time factors. Singh et al. [16] studied the formation mechanism and prediction method of surface subsidence basins. By analyzing the surface subsidence at the edge of the goaf and the stability of the gully slope, Li et al. [17] determined the principle of the subsection reinforcement of the gully slope under the dynamic influence of coal seam mining. Li et al. [18] used the FLAC3D5.0 program to simulate the evolution law of the overburden strata under the coal mining conditions of the study area. A mathematical model was established to predict the settlement range and displacement of the surface after coal mining. Deng et al. [19] used numerical simulation to determine the surface subsidence boundary and surface collapse volume after mining in the study area. In order to accurately predict the surface subsidence of the mining area, Cheng et al. [20] established a surface subsidence prediction model based on the influence function method. Sun et al. [21] used theoretical analysis and numerical simulation (FLAC3D5.0) to determine the coal pillar and mining widths, and to discuss the coal pillar stress distribution and surface subsidence for different mining scenarios. Chen et al. [22], based on the geomorphology, examined the chained principle for the development of the collapse in Mt. Focusing on falling perilous rocks, Tang et al. [23,24] established a method to calculate the combined stress intensity factor of the dominant fissure under the falling excitation action of perilous rock. At present, obvious deficiencies remain in the research on the special situation of perilous rock above the coal mine goaf. In view of this, in this study, the research object was the surface perilous rock of a mining area in Guizhou Province, China, and the collapse of perilous rock above the coal mine goaf was examined. By investigating the geological conditions of coal mines and the scope, scale, and shape of the perilous rock belt, this study examined the stability of the overlying strata affected by mining, and analyzed the factors affecting the stability of perilous rock, which is of great significance to the safe and efficient production of a coal mine.

## 2. Coal Mine Risk Situation

Perilous rock refers to structural planes of rock mass on steep cliffs or slopes cutting each other at large angles. In addition, gravity, weathering, earthquakes, heavy rains, or artificial engineering activities can lead to instability and underdevelopment of the rock mass, which is otherwise in a stable or limit equilibrium state. The strata in the Panjiang mining area in China are monoclinic, and mainly composed of ridge mountains of erosion and dissolution. Affected by the lithology of strata, cliffs are formed locally, and the overall terrain is uneven, with large joint cutting. The geographical coordinates of the studied coal mines are as follows:  $106^{\circ}53'49''$ – $106^{\circ}54'25''$  east longitude;  $28^{\circ}30'14''$ – $28^{\circ}31'32''$  north latitude. By observing whether there are obvious cracks in the rock area, and whether the cracks were continuously lengthened, widened, or increased, it was determined that the perilous rock belt is distributed on the cliff on the northern side of the mining industrial square. The shortest distance between the industrial square and the perilous rock belt is about 55 m, and the total length of the perilous rock belt is about 400 m. The terrain is high in the northwest and low in the southeast, and the height difference is within 145–159 m. According to a field investigation and the analysis of collected data, the perilous rock threatening the coal mine industrial square ranges from southeast to northwest, and was assigned division numbers of W1, W2, W3, W4, W5, W6, and W7. The specific distribution of the perilous rock is shown in Figure 1.

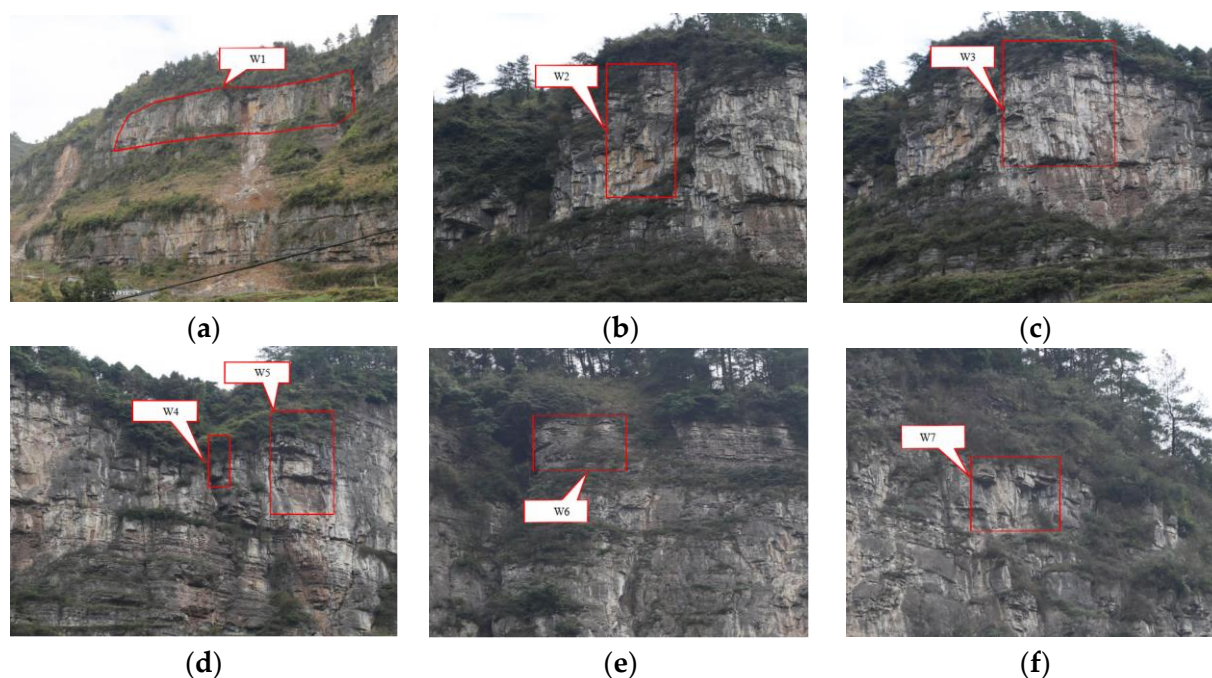


**Figure 1.** Profile of perilous rock. (a) W1 perilous rock; (b) W2 perilous rock; (c) W3 perilous rock; (d) W4, W5 perilous rock; (e) W6 perilous rock; (f) W7 perilous rock.

The details of the scope, scale, and shape of the perilous rock are shown in Table 1.

**Table 1.** Statistical table of morphological characteristics of collapse.

Numbered	Length (m)	Thickness (m)	Height (m)	Scale and Morphological Characteristics
W1	240	2.5–35	32–38	W1 is located at the end of the northwest side of the entire perilous rock belt, the cracks in the posterior wall have penetrated the whole perilous rock mass, and some stones are suspended on the perilous rock mass.
W2	14–17	1.3–16	32.5	W2 is adjacent to the W1 perilous rock mass, about 15 m apart; the lower part of the perilous rock mass has undergone a block phenomenon, and the debris is a broken block.
W3	19–21	3–3.5	50	W3 is adjacent to the W2 perilous rock mass, and the perilous rock is massive. The steeply inclined fractures on both sides of the perilous rock mass develop and penetrate the whole perilous rock mass.
W4	1.5	2	3	W4 is developed in the wedge formed by the mutual cutting of the two fractures. The lower part of the wedge has broken away from the parent rock, and the remaining part is suspended in the two fractures.
W5	8–10	1.5–3	20–25	W5 is about 10 m from the W3 perilous rock mass. The perilous rock mass is mainly fragmented, and the lower part has collapsed, resulting in the hanging of the upper perilous rock mass.
W6	10	3	6.5	W6 is located at the top of the perilous rock belt. The perilous rock mass is broken into pieces, and there is a drop at the bottom of the perilous rock mass.
W7	12	0.5–1	10	W7 is located at the end of the southeast side of the perilous rock belt, the lower part is controlled by joint fissures to form a wedge, and the rock mass at the bottom has collapsed from the parent rock.

### 3. Stability Evaluation of Perilous Rock

#### 3.1. Macroscopic Analysis of the Stability of Perilous Rock

A stereographic projection is a software-based approach used to judge the stability of a slope [25,26]. Using the geological occurrence of the plane and straight line obtained in the field, the relevant parameters of the related inclination can be obtained. Using the angular

distance relationship, the perilous rock in the study area is reflected in the projection plane for analysis and processing, and the stability of perilous rock is preliminarily judged. This method can simplify the complicated calculation process, and has the advantages of being intuitive and convenient.

The macro-analysis of the W1 perilous rock mass was undertaken mainly to evaluate the overall stability of the perilous rock. According to the field investigation, there are three groups of joint cracks in the perilous rock zone of the coal mine industrial square. The relevant physical parameters are shown in Table 2:

**Table 2.** Collapsed perilous rock belt of the coal mine industry square.

Numbered	Strike (°)	Tendency (°)	Dip Angle (°)	Word Hole (mm)	Density (g/cm <sup>3</sup> )	Filling Condition	Weathering of Crack Surface
P	340	330	27				
L1	330	72	15	300–500	2.85	No fillings	Strong to medium weathering
L2	100	251	80	200–500	2.82	No fillings	Strong to medium weathering
L3	80	188	69	100–300	2.74	Filled with clay and mudstone	Strong to medium weathering

There are three groups of joint fissures in the perilous rock zone: ① 330°∠27°; ② 72°∠15°; ③ 251°∠80°. Through field investigation, considering the scale form of the perilous rock mass, the geological analogy method was used to judge its stability from a macro perspective. The stereographic projection analysis is shown in Figure 2 below.

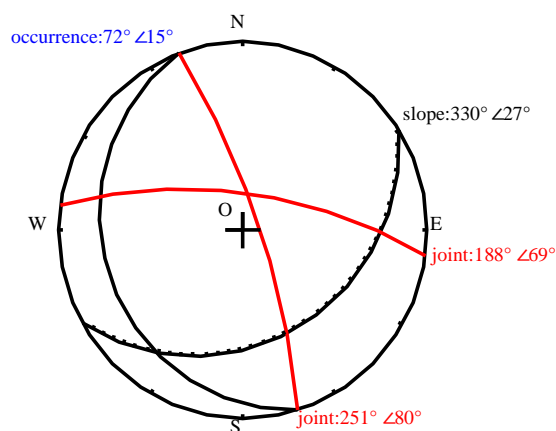


**Figure 2.** Diagram of the stereographic projection.

The analysis from the planar projection is as follows:

(1) Slope and rock occurrence analysis: From the tendency analysis, the slope inclination is 330° and the rock occurrence tendency is 72°. The inclination of the slope surface in this perilous rock zone is nearly 90° orthogonal to the attitude of the rock stratum, so the inclination of the rock stratum is conducive to the stability of the slope, and the attitude of the rock stratum belongs to the stable structural plane. From the angle analysis, the slope angle is 27° and the attitude angle of rock stratum is 15°. The dip angle of the rock is less than the slope foot, so there is no support point on the slope surface, and the rock layer at this time is not conducive to slope stability.

(2) Joint analysis: There are two groups of joints in the slope, with joint 1 having an inclination of 251°, inclination of 80°, and joint 2 having an inclination of 188°, inclination of 69°. The intersection point of joints 1 and 2 is located on the opposite side of the stereographic projection arc surface of the slope. The inclination of the combined intersection line is approximately opposite to that of the slope, so the combined surface is conducive to

slope stability. At the same time, joint 1 tends to be the main sliding direction, and joint 2 is the cutting surface. It is easier for the slope to produce more perilous rock monomers along the structural surface of joint 2.

The analysis shows that the perilous rock zone of the slope is in a relatively stable state as a whole.

### 3.2. Computational Model and Formula

The stability calculation of the perilous rock mass mainly adopted the method of field investigation and checking of the formula calculation. After analyzing the main stress conditions of the perilous rock mass, the perilous rock in the field was preliminarily classified. In addition to the main instability deformation and failure mode, the small blocks in the perilous rock zone are mostly scattered stones. The W4 perilous rock mass belongs to the dumping model, and the remainder belong to the falling model.

(1) The calculation model of dumping perilous rock is shown in Figure 3.

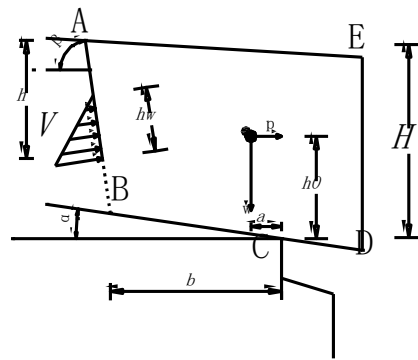


Figure 3. Calculation model of dumping perilous rock.

This model is considered according to the unit width without considering the tensile strength of the base. Point C is taken as the overturning point, which is the weathering outer edge point in the base rock. Then, the stability factor is:

① When the tensile strength of the trailing edge rock mass is controlled, it is calculated according to the following formula:

A: perilous rock weight heart outside the tipping point.

$$F = \frac{M_R}{M_O} = \frac{\frac{1}{2} f_{lk} \cdot \frac{H-h}{\sin \beta} \left[ \left( \frac{2(H-h)}{3 \sin \beta} \right) + \frac{b}{\cos \alpha} \cos(\beta - \alpha) \right]}{W_a + p_b + V \left[ \frac{h_w}{3 \sin \beta} + \frac{H-h}{\sin \beta} + \frac{b}{\cos \alpha} \cos(\beta - \alpha) \right]} \quad (1)$$

B: The center of gravity of the perilous rock mass is within the overturning point, which may be C.

$$F = \frac{M_R}{M_O} = \frac{\frac{1}{2} f_{lk} \cdot \frac{H-h}{\sin \beta} \left[ \frac{2(H-h)}{3 \sin \beta} + \frac{b}{\cos \alpha} \cos(\beta - \alpha) \right] + W_a}{p h_0 + V \left[ \frac{h_w}{3 \sin \beta} + \frac{H-h}{\sin \beta} + \frac{b}{\cos \alpha} \cos(\beta - \alpha) \right]} \quad (2)$$

In the formula:

$F$ : Stability coefficient;

$H_w$ : Water filling height of trailing edge fracture (m);

$h$ : Fracture depth of trailing edge (m);

$H$ : Vertical distance from top of trailing edge fracture to bottom of unpenetrated section (m);

$F_{lk}$ : Standard tensile strength of the perilous rock mass (MPa);

$a$ : Horizontal distance from body weight center of perilous rock to overturning point;

$b$ : Horizontal distance from bottom of unpenetrated section of trailing edge fracture to overturning point;

$h_0$ : Vertical distance from perilous rock mass center to overturning point;  
 $\alpha$ : Inclination angle of contact surface between perilous rock mass and base ( $^\circ$ );  
 $\beta$ : Inclination angle of trailing edge fracture ( $^\circ$ );  
 $P$ : seismic force (KN/m);  
 $V$ : cleft water pressure (KN/m).

② When the tensile strength of the bottom rock mass is controlled, it is calculated according to the following formula:

$$F = \frac{\frac{1}{3}f_{lk}b^2 + W_a}{ph_0 + V\left(\frac{h_w}{3\sin\beta} + b\cos\beta\right)} \quad (3)$$

In the formula:

$F$ : Stability coefficient;

$f_{lk}$ : Standard tensile strength of perilous rock mass (MPa);

$H_w$ : Water filling height of trailing edge fracture (m);

$a$ : Horizontal distance from body weight center of perilous rock to overturning point;

$b$ : Horizontal distance from bottom of unpenetrated section of trailing edge fracture to overturning point;

$h_0$ : Vertical distance from perilous rock mass center to overturning point;

$\alpha$ : Inclination angle of contact surface between perilous rock mass and base ( $^\circ$ );

$\beta$ : Inclination angle of trailing edge fracture ( $^\circ$ );

$P$ : seismic force (KN/m);

$V$ : cleft water pressure (KN/m).

(2) The falling perilous rock calculation model is shown in Figure 4, according to the unit width considerations in the following formula:

$$F = \frac{(W \cos \beta - p \sin \beta - V) \tan \beta + c \frac{h}{\sin \beta}}{W \sin \beta + p \cos \beta} \quad (4)$$

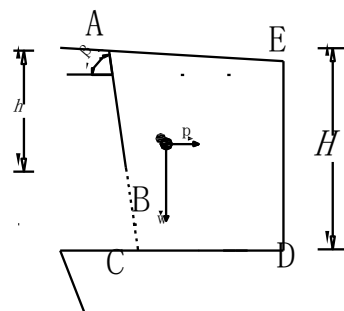


Figure 4. Stability calculation model of falling perilous rock.

In the formula:

$F$ : Stability coefficient;

$\alpha$ : Inclination angle of contact surface between perilous rock mass and base ( $^\circ$ );

$\beta$ : Inclination angle of trailing edge fracture ( $^\circ$ );

$\varphi$ : Standard value of internal friction angle of trailing edge cracks ( $^\circ$ );

$h$ : Fracture depth of trailing edge (m);

$P$ : Seismic force (KN/m);

$W$ : Gravity of perilous rock mass (KN/m). According to  $\gamma \times S$ ;

$V$ : cleft water pressure (KN/m);

$C$ : Standard value of cohesion of trailing edge fracture (MPa).

### 3.3. Stability Calculation and Evaluation

The stability calculation and support design of the perilous rock mass do not consider the seismic action [27]. The stability calculation of the perilous rock mass in the working area during an earthquake mainly adopts the following two working conditions, and considers the reduction in the shear strength index of the rock mass structural plane under rainstorm conditions:

Condition 1: dead weight + cleft water pressure (water filling height is calculated according to 1/3 fracture height).

Condition 2: dead weight + cleft water pressure (in the case of a one-in-20-year rainstorm, water filling height is calculated according to 1/2 crack height).

According to the ‘China landslide prevention engineering survey specification’ (DZ/T 0218-2006), the slope stability coefficient was determined as shown in Table 3.

**Table 3.** Criteria for classification of the stability state of a perilous rock mass.

MODE of Failure	Stable State of Perilous Rock			
	Destabilization	Not Stable	Basically Stable	Stable
dumping type	$F < 1.0$	$1.00 \leq F < 1.5$	$1.5 \leq F < 1.8$	$F \geq 1.8$
falling type	$F < 1.0$	$1.00 \leq F < 1.3$	$1.3 \leq F < 1.5$	$F \geq 1.5$

According to the above stability calculation formula, the stability of the perilous rock monomer and perilous rock belt was calculated, and the parameters are shown in Table 4.

**Table 4.** Stable value parameters.

Stability Parameter	W1		W2		W3		W4		W5		W6		W7	
	①	②	①	②	①	②	①	②	①	②	①	②	①	②
<i>H</i>	16.3	16.3	32.5	32.5	50	50	1.5	1.5	22.5	22.5	6.5	6.5	10	10
<i>h</i>	10.3	10.3	11.9	11.9	6.7	6.7	0.38	0.75	1.5	1.5	3.8	3.8	1.2	1.2
<i>A<sub>0</sub></i>	0.78	0.78	1.13	1.13	2.57	2.57	0.53	0.53	2.14	2.14	0.5	0.5	2.27	2.27
<i>B<sub>0</sub></i>	9.2	9.2	18.02	18.02	28.68	28.68	1.5	1.5	13.67	13.67	4.5	4.5	11.8	11.8
<i>F<sub>tk</sub></i>	600	600	600	600	600	600	600	600	600	600	600	600	600	600
<i>c</i>	120	80	120	80	120	80	120	80	120	80	120	80	120	80
<i>Φ</i>	32.1	30	32.1	30	32.1	30	32.1	30	32.1	30	32.1	30	32.1	30
<i>ζ</i>	0.15	0.15	0.15	0.15	0.15	0.15			0.15	0.15	0.15	0.15	0.15	0.15
<i>p</i>	0	0	0	0	0	0	0	0	0	0	0	0	0	0
<i>S</i>	19.2	19.2	72.5	72.5	155.8	155.8			75.98	75.98	7.98	7.98	30.26	30.26
<i>V</i>							1.7	1.7						
<i>W</i>							161	161						
<i>sinβ</i>							1	1						
<i>cosα</i>							1	1						
<i>cos(β - α)</i>							0.2	0.2						
<i>F</i>	1.39	1.16	1.27	32.5	1.31	1.03	1.38	1.16	1.23	1.03	1.51	1.26	1.35	1.07

*H*: Vertical distance from upper part of trailing edge fracture to lower part of unpenetrated section (m); *h*: Fracture depth of trailing edge (m); *A<sub>0</sub>*: Horizontal distance from body weight center of perilous rock to potential failure surface (m); *B<sub>0</sub>*: The plummeting distance from the weight center of perilous rock to the centroid of potential damaged surface (m); *F<sub>tk</sub>*: Standard for Tensile Strength of perilous rock mass (MPa); *c*: Standard value of cohesion of perilous rock mass (MPa); *Φ*: Standard value of cohesion of perilous rock mass (°); *ζ*: Calculation coefficient of bending moment of perilous rock; *p*: seismic force (KN/m); *S*: Single width area of perilous rock mass (m<sup>2</sup>); *α*: Angle of contact surface between perilous rock mass and base (°); *β*: Inclination angle of trailing edge fracture (°); *V*: cleft water pressure (KN/m); *W*: Gravity of perilous rock mass (KN/m); *F*: stability factor.

The quantitative calculation using the formulas was carried out for the models established for the falling perilous rock and the dumping perilous rock, respectively. The calculation results are shown in Table 5.

**Table 5.** Calculation results of the stability of the perilous rock mass.

Numbered	Mode of Failure	Calculated Work Condition	Saturated Uniaxial Compressive Strength (MPa)	Stability Factor	Steady-State
W1	falling type	1	38.50	1.39	basically stable
		2		1.16	not stable
W2	falling type	1	51.20	1.27	not stable
		2		1.16	not stable
W3	falling type	1	44.70	1.31	basically stable
		2		1.03	not stable
W4	dumping type	1	39.20	1.38	basically stable
		2		1.16	not stable
W5	falling type	1	50.10	1.23	not stable
		2		1.03	not stable
W6	falling type	1	47.30	1.51	stable
		2		1.26	not stable
W7	falling type	1	39.40	1.35	basically stable
		2		1.07	not stable

#### 4. Numerical Simulation Analysis of Perilous Rock Stability under Mining Influence

##### 4.1. Model Establishment

The perilous rock studied in this paper has two types: falling type and dumping type. Because the W6 perilous rock is in a stable state, the remainder of the perilous rock is basically either stable and unstable. Therefore, the simulation used the W6 stable perilous rock as the research object to judge the influence of coal seam mining on the W6 perilous rock. The numerical model established a two-dimensional model of coal seam mining at the location of perilous rock W6 as a section. The boundary conditions of this study were determined according to the actual situation. The bottom and both sides of the model are zero displacement boundary conditions. The upper part of the model and the perilous rock are free boundaries, which are mainly subject to gravity stress. The gravity stress of the original rock is applied on the upper boundary [28,29], and the gradient horizontal stress is applied on the left and right boundaries of the model. Due to the small dip angle of the coal seam, the horizontal model was established as follows:

The model uses the horizontal direction as the X-axis, and the total length in the X-axis direction is 450 m. The Y-axis is along the vertical direction and the total thickness of the Y-axis is 240 m. The model has 11 inflection points, which, in the clockwise direction are (0, 0), (0, 102), (11.73, 111.82), (60.84, 133.45), (87.37, 150), (103.98, 153.36), (111.48, 228.45), (110.52, 240), (112.56, 240), (450, 240), (450, 0). The crack command was used to connect the coordinate primaries between the points with straight lines. the position of the coal seam and stratum lithology is marked in Figure 5:

The numerical simulation using the Mohr–Coulomb yield rule is:

$$f = \sigma_1 - \sigma_3 \frac{1 + \sin \varphi}{1 - \sin \varphi} = 2c \sqrt{\frac{1 - \sin \varphi}{1 + \sin \varphi}} \quad (5)$$

where:

$\sigma_1$ : maximum principal stress (MPa);

$\sigma_3$ : minimum principal stress (MPa);

$c$ : cohesive force (MPa);

$\theta$ : angle of internal friction ( $^\circ$ ).

The physical and mechanical parameters of each rock mass are shown in Table 6.

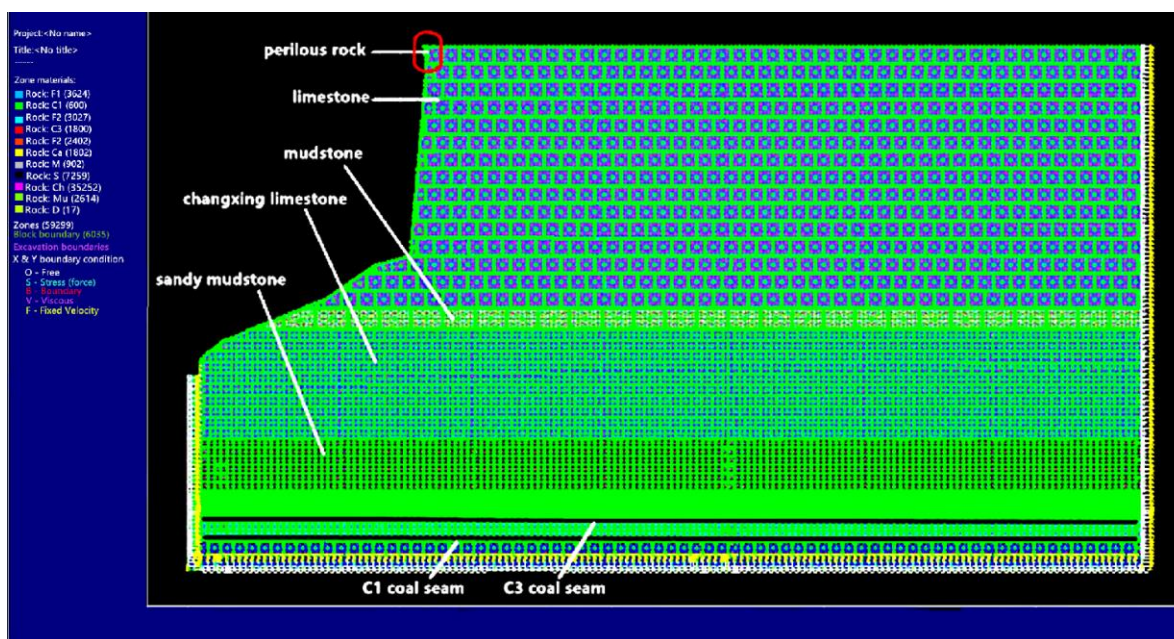


Figure 5. UDEC calculation model (angle 0°).

Table 6. Physical and mechanical parameters of rock mass.

Number	Rock Type	Thickness / (m)	Density / (g/cm <sup>3</sup> )	Bulk Modulus / (GPa)	Shear Modulus / (GPa)	Friction Angle / (°)	Cohesion / (MPa)	Tensile Strength / (MPa)
1	limestone	110	2.80	5.57	4.53	38	11.4	6.7
2	mudstone	10	2.70	2.86	1.4	39	2.8	2.48
3	Changxing limestone	50	2.43	11.1	8.3	35	2.4	4.4
4	sandy mudstone	24	2.25	10.2	6.1	30	1.8	3.2
5	mudstone	4	2.55	5.8	3.2	30	1.2	3.25
6	sandy mudstone	4.5	2.25	10.2	6.1	30	1.8	3.2
7	carbon mudstone	1.5	2.45	4.3	2.8	30	0.7	1.8
8	C3 coal	2	1.47	1.19	0.82	25	1.3	1.79
9	Clay rock	10	2.25	4.39	2.27	27	4.9	3.8
10	C1 coal	1	1.47	1.19	0.82	25	1.3	1.79
11	mudstone	13	2.55	5.8	3.2	30	1.2	3.25

#### 4.2. Analysis of Numerical Simulation Results

The two-dimensional model of C3 coal seam mining was established by taking the location of the W6 perilous rock mass as the section to carry out the numerical simulation. According to the mining conditions of the C3 coal seam in the coal mine studied in this paper, 50 m coal pillars were placed at the left and right ends, and the simulation was carried out in 50 m units in front of the working face to accurately represent the mining situation of the C3 coal seam in the coal mine. According to the simulation results, two kinds of fractures occurred in the simulation: separated fractures and broken fractures [30].

As shown in Figure 6a, when the working face is mined to 50 m, coal mining only leads to local cracks above the goaf of the working face, which has little effect on the overlying strata far from the coal seam. When the working face is mined to 100 m, the fracture is still located above the goaf as a whole, but its development range is larger. The transverse separation fracture and longitudinal separation fracture are connected, and the fracture continues to develop upward, but it has little effect on the surface perilous rock, as shown in Figure 6b. When the working face advances to 150 m, due to the continuous mining, the fracture at this time has developed to the position close to the surface; however, it has not yet been connected with the surface, and is at a distance of about 10 m from the surface. At this time, the fracture is still far from the surface perilous rock, and has little influence on the perilous rock, as shown in Figure 6c. When the working face advances to

200 m, as the coal seam continues to be excavated, the fractures continue to develop in the direction toward the working face. The previous fracture zone continues to be compacted, and new fracture zones appear. At this time, above the position of mining at about 200 m, there are separate cracks connecting with the surface, and there are also upward cracks in the adjacent position. The surface at this position has shown obvious subsidence, but the influence of mining on the perilous rock mass has not been seen, as shown in Figure 6d. When the working face advances to 250 m, the fracture continues to develop in the direction of mining. At this time, the fracture is about 50 m from the horizontal distance of the goaf, and there is a local fracture at 10–40 m below the corner of the slope. This fracture is not connected with the previous fracture, and the fracture is located directly below the perilous rock. If the mining is continued, the fracture will have a great impact on the surface perilous rock. When the working face advances to 300 m, as the mining advances to the lower right side of the perilous rock, the rock strata in the goaf have fully collapsed, and collapsed to the floor with the advance in mining. The surface also has different degrees of depression. The rock strata have obvious vertical fracture cracks, and there are many fractures above the goaf and coal wall. The mining has a significant impact on the overlying strata, and the upper rock strata of the roof are greatly affected by the mining. At this point, the cracks at the foot of the slope and above the goaf have been partially penetrated, and the cracks are close to the perilous rock as a whole, as shown in Figure 6f. When the working face is advanced to 350 m, the fracture has penetrated with the surface of the perilous rock, and the perilous rock has not yet collapsed. However, the existence of the fracture has an extremely unfavorable impact on the stability of the perilous rock, as shown in Figure 6g.

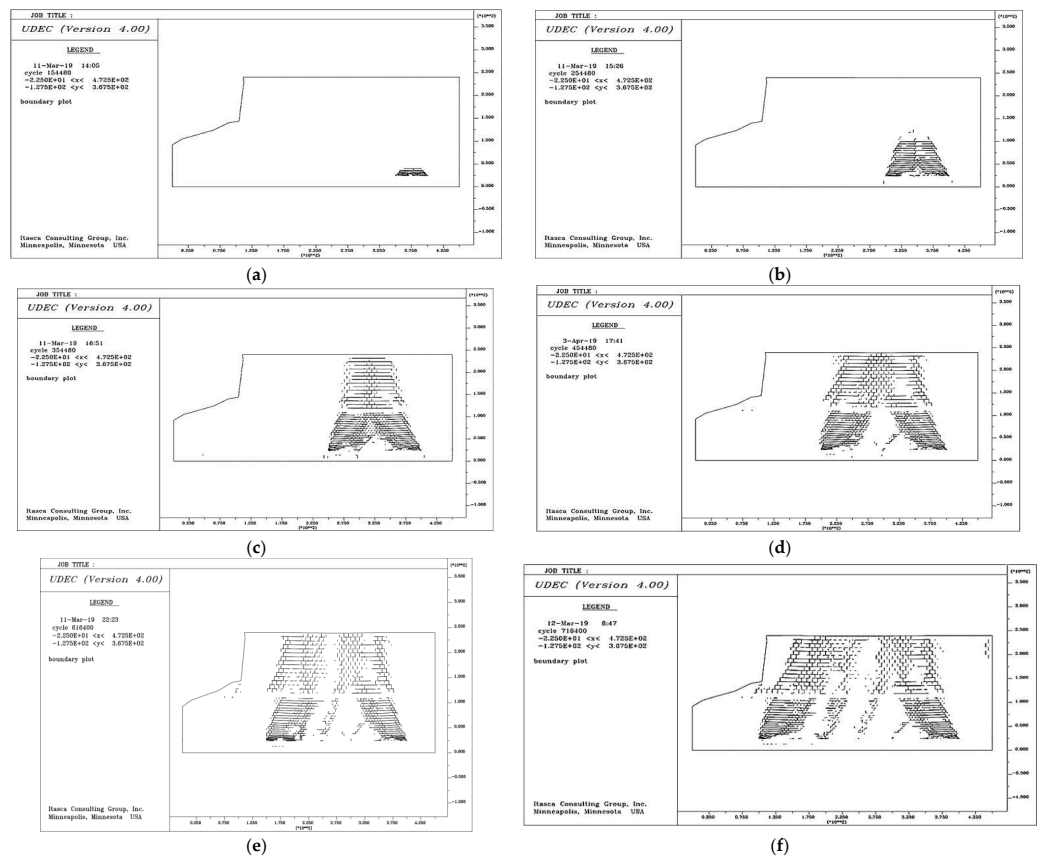
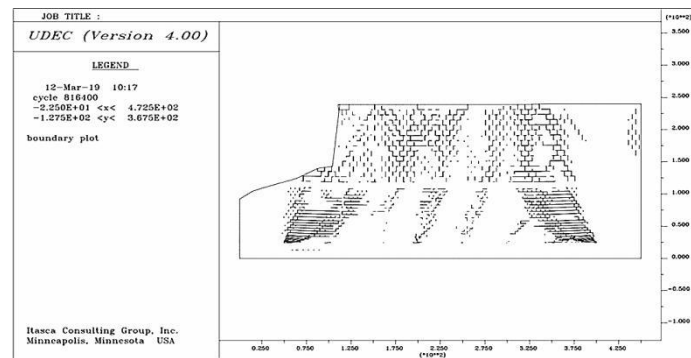


Figure 6. Cont.



(g)

**Figure 6.** Coal seam mining effect diagram: (a) 50 m forward; (b) 100 m forward; (c) 150 m forward. (d) 200 m forward: separated fissure and surface penetration; (e) 250 m forward; (f) 300 m forward: the whole crack is close to the perilous rock; (g) 350 m forward: fracture and surface penetration of perilous rock.

### 5. Stability Control of Surface Perilous Rock

The surface perilous rock mass is cut by multiple sets of structural planes. The intersections of the cracks, weak layers, and faults in the rock mass determine the diversity of the failure mode of the perilous rock mass, and are the reasons for the complexity of the failure and instability. Liu et al. [31] explained the dynamic source of the failure mode of the perilous rock mass, and proposed that the main driving force of the collapse is the apparent sliding force outward from the slope. The apparent sliding force outward from the slope can overcome the shear resistance of the front edge of the perilous rock mass and the friction of the bottom surface. Xie [32] et al. analyzed the influence of mining activities on the structure and mechanical parameters of the overlying rock mass, and proposed the evaluation standard and basis for the safety degree of the cavity overlying rock mass. Aref [33] et al. proposed a flexible network locking method with an obvious effect on the treatment of the perilous rock mass, and comprehensively outlined the design principle of the flexible network locking method. Therefore, the stability control of surface perilous rock mass can be considered from two aspects of underground coal mining and surface disaster management. The mining situation of the C3 coal seam was numerically simulated by UDEC software, and the fracture of the overlying strata and the collapse of the surface perilous rock mass were theoretically analyzed. The trajectory of the perilous rock collapse was numerically simulated using Rockfall software, and the simulation was carried out from underground and at the surface. However, the actual surface collapse of the perilous rock is not only affected by coal mining, but is also related to many factors [34–38]. In addition, theoretical speculation about the range of influences on the collapse will also deviate to a certain degree from the actual situation.

Using the “support” method to set up coal pillars in the UDEC numerical simulation, the following method was finally determined to have the best mining effect: the C3 coal seam working face is pushed from right to left, with 45 m permanent protective coal pillars left at both ends, and 15 m local protective coal pillars left at 60 m. Because the UDEC software only simulates the two-dimensional plane, the width of the coal pillar can only be determined according to the field equipment. In addition, it is necessary to ensure that coal mining-related equipment can pass through the coal pillar. Finally, the simulated UDEC fracture development diagram is shown in Figure 7. For the perilous rocks W1, W2, W3, W4, W5, W6, and W7 on the surface, and the loose structure on the slope, artificial and mechanical methods can be used to remove the rock according to the current crack development of the rock mass, and the stones formed by the cutting can be transported outside and stacked at the designated location. In addition, an SNS active protection network can be used to protect the whole perilous rock belt. In this method of mining, the

final fracture development is basically below the Changxing limestone section, and will not involve the surface and perilous rock.

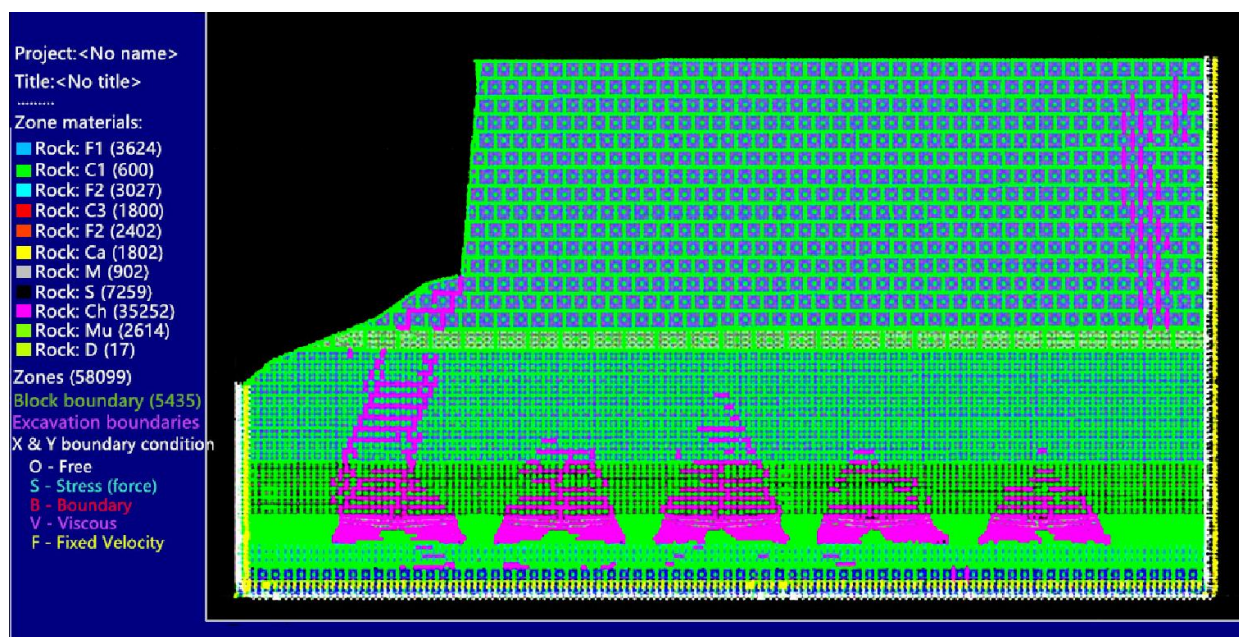


Figure 7. Diagram showing the effect of leaving a partial coal pillar.

## 6. Conclusions

(1) The perilous rock is basically stable without the influence of mining. The analysis of the fracture development obtained by the simulation shows that, with the mining of the C3 coal seam, the fracture of the upper strata starts to develop to the surface. The fracture gradually runs through the surface and finally causes a longitudinal separation fracture at the perilous rock. Due to the existence of the fracture, the perilous rock has a downward shear force, resulting in the collapse of the rock.

(2) The stability of the surface perilous rock mass is largely affected by the influence of underground coal mining. Through the study of the development of perilous rock fractures in the process of mining, it was concluded that when 45 m permanent protective coal pillars are left at both ends, and 15 m local protective coal pillars are left at 60 m, the safety of coal mining can be ensured and the surface and perilous rock will not be affected.

(3) The underground mining of a coal mine involves complex system engineering. In this study, UDEC software was used to simulate the influence of coal seam mining on the surface perilous rock collapse. The development of fractures was only analyzed from the two-dimensional perspective. This helps determine the significant effect of mining on the perilous rock collapse, but the weights of the influences cannot be reflected in the analysis. At present, this analysis remains in the theoretical stage, and the specific effects need to be further verified.

**Author Contributions:** Conceptualization, L.G. (Lu Gao) and X.K.; methodology, L.G. (Lin Gao); software, Z.M.; validation, Z.M., X.K. and L.G. (Lin Gao); formal analysis, X.K.; investigation, X.K.; resources, X.K.; data curation, L.G. (Lu Gao); writing—original draft preparation, L.G. (Lu Gao); writing—review and editing, X.K.; visualization, X.K.; supervision, L.G. (Lin Gao); project administration, L.G. (Lin Gao); funding acquisition, X.K. and L.G. (Lin Gao). All authors have read and agreed to the published version of the manuscript.

**Funding:** National Natural Science Foundation of China (No. 52064009; 52004073); Guizhou Science and Technology Fund Project (Qiankehe Foundation [2020] 1Y216).

**Data Availability Statement:** The data presented in this study are available on request from the corresponding author.

**Conflicts of Interest:** The authors declare no conflict of interest.

## References

1. Mu, C.; Yu, X.Y.; Zhao, B.C. The Formation Mechanism of Surface Landslide Disasters in the Mining Area under Different Slope Angles. *Adv. Civ. Eng.* **2021**, *2021*, 106–119. [[CrossRef](#)]
2. Li, H. Artificial Intelligence and Internet of Things (IoT) in Civil Engineering. *Adv. Civ. Eng.* **2021**, *2021*, 111–123.
3. Hungr, O.; Leroueil, S.; Picarelli, L. The Varnes classification of landslide types, an update. *Landslides* **2014**, *11*, 167–194. [[CrossRef](#)]
4. Liu, C.; Zhang, S.; Ding, L.; Liao, J. Identification of perilous rock mass of high slope and study of anchoring method based on laser scanning. *Chin. J. Rock Mech. Eng.* **2012**, *31*, 2139–2146.
5. Crosta, G.B.; Agliardi, F. Parametric calculation of 3D dispersion of rockfall trajectories. *Nat. Hazards Earth Syst. Sci.* **2004**, *4*, 583–598. [[CrossRef](#)]
6. Geng, J.B.; Li, Q.H.; Li, X.S.; Zhou, T.; Liu, Z.; Xie, Y. Research on the evolution characteristics of rock mass response from open-pit to underground mining. *Adv. Mater. Sci. Eng.* **2021**, *2021*, 3200906. [[CrossRef](#)]
7. Kong, D.Z.; Cheng, Z.; Zheng, S. Study on failure mechanism and stability control measures in large-cutting-height coal mining face with deep-buried seam. *Bull. Eng. Geol. Environ.* **2021**, *78*, 6143–6157. [[CrossRef](#)]
8. Bui, D.T.; Tuan, T.A.; Klempe, H.; Pradhan, B.; Revhaug, I. Spatial prediction models for shallow landslide hazards: A comparative assessment of the efficacy of support vector machines, artificial neural networks, kernel logistic regression, and logistic model tree. *Landslides* **2016**, *13*, 361–378.
9. Cao, Z.Z.; Ren, Y.L.; Wang, Q.T. Evolution Mechanism of Water-Conducting Channel of Collapse Column in Karst Mining Area of Southwest China. *Geofluids* **2021**, *2021*, 6630462. [[CrossRef](#)]
10. Chen, H.K.; Tang, H.M.; Wang, R. Calculation method of stability for perilous rock and application to the three gorges reservoir. *Chin. J. Rock Mech. Eng.* **2004**, *23*, 614–619. [[CrossRef](#)]
11. Hou, P.; Liang, X.; Gao, F.; Dong, J.B.; He, J.; Xue, Y. Quantitative visualization and characteristics of gas flow in 3D pore-fracture system of tight rock based on Lattice Boltzmann simulation. *J. Nat. Gas Sci. Eng.* **2021**, *89*, 103867. [[CrossRef](#)]
12. Liang, X.; Hou, P.; Xue, Y.; Yang, X.J.; Gao, F.; Liu, J. A fractal perspective on fracture initiation and propagation of reservoir rocks under water and nitrogen fracturing, Fractals-Complex Geom. *Patterns Scaling Nat. Soc.* **2021**, *29*, 7.
13. Qian, M.G.; Miao, X.X.; Xu, J.L. Theoretical study of key stratum ground control. *J. China Coal Soc.* **1996**, *21*, 225–230.
14. Xu, J.L.; Qian, M.G.; Zhu, W.B. Study on influences of primary key stratum on surface dynamic subsidence, *Chin. Rock Mech. Rock. Engl.* **2005**, *24*, 787–791.
15. Baryak, A.A.; Telegin, E.A.; Samodelkina, N.A. Prediction of the Intensive Surface Subsidence in Mining Potash Series. *J. Min. Sci.* **2005**, *41*, 312–319. [[CrossRef](#)]
16. Singh, K.B. Pot-hole Subsidence in Son-Mahanadi master Coal Basin. *Eng. Geol.* **2007**, *89*, 88–97. [[CrossRef](#)]
17. Li, J.W.; Li, X.T.; Liu, C.Y. Dynamic Changes in Surface Damage Induced by High-Intensity Mining of Shallow, Thick Coal Seams in Gully Areas. *Adv. Civ. Eng.* **2020**, *2020*, 246–262. [[CrossRef](#)]
18. Li, G.; Yang, Q.H. Prediction of Mining Subsidence in Shallow Coal Seam. *Math. Probl. Eng.* **2020**, *2020*, 339–404.
19. Deng, X.; Li, L.; Tan, Y. Numerical simulation of surface subsidence induced by underground mining in mines. *Saf. Coal Mines* **2018**, *49*, 188–192.
20. Cheng, J.W.; Zhao, G.; Li, S.Y. Predicting Underground Strata Movements Model with Considering Key Strata Effects. *Geotech. Geol. Eng.* **2018**, *36*, 621–640. [[CrossRef](#)]
21. Sun, W.; Zhang, Q.; Luan, Y.Z. A study of surface subsidence and coal pillar safety for strip mining in a deep mine. *Environ. Earth Sci.* **2018**, *77*. [[CrossRef](#)]
22. Chen, H.K.; Tang, H.M.; Xian, X.F. Developing Mechanism for Collapse Disaster in Rocky Mountain Area—Taking Mt. Hongyan in the National Scenic Spots of Simianshan as an Example. *Adv. Eng. Sci.* **2010**, *42*, 1–6.
23. Tang, H.M.; Wang, Z.; Chen, H.K.; Xian, X.F. Contribution ratio of excitation action triggered by collapse of perilous rock to stability of perilous rock. *J. Vib. Shock* **2012**, *31*, 32–37.
24. Tang, H.M.; Wang, Z.; Xian, X.F.; Chen, H.K. Violent-slide rock avalanche and excitation effect of perilous rock. *J. Chongqing Univ.* **2011**, *34*, 32–37.
25. Zheng, J.; Lu, Q.; Deng, J.; Yang, X.; Fan, X.; Ding, Z. A modified stereographic projection approach and a free software tool for kinematic analysis of rock slope toppling failures. *Bull. Eng. Geol. Environ.* **2019**, *78*, 4757–4769. [[CrossRef](#)]
26. Kincal, C. Application of two new stereographic projection techniques to slope stability problems. *Int. J. Rock Mech. Min. Sci.* **2014**, *66*, 136–150. [[CrossRef](#)]
27. Li, X.S.; Liu, Z.F.; Yang, S. Similar physical modeling of roof stress and subsidence in room and pillar mining of a gently inclined medium-thick phosphate rock. *Adv. Civ. Eng.* **2021**, *2021*, 6686981. [[CrossRef](#)]
28. Ren, W.Z.; Guo, C.M.; Peng, Z.Q.; Wang, Y.G. Model experimental research on deformation and subsidence characteristics of ground and wall rock due to mining under thick overlying terrane. *Int. J. Rock Mech. Min. Sci.* **2010**, *47*, 614–624. [[CrossRef](#)]
29. Wu, H.; Ma, D.; Spearing, A.J.S.; Zhao, G.Y. Fracture phenomena and mechanisms of brittle rock with different numbers of openings under uniaxial loading. *Geomech. Eng.* **2021**, *25*, 481–493.
30. Ma, D.; Kong, S.B.; Li, Z.H.; Zhang, Q.; Wang, Z.H.; Zhou, Z.L. Effect of wetting-drying cycle on hydraulic and mechanical properties of cemented paste backfill of the recycled solid wastes. *Chemosphere* **2021**, *282*, 131163. [[CrossRef](#)]

31. Liu, C.Z. Formation and Collapse Cause Analysis of Jiweishan perilous rock Mass in Wu long, Chongqing. *J. Eng. Geol.* **2010**, *18*, 297–304.
32. Xie, Q.D.; Ding, X.P. Dynamic Analysis of Rock Mass Stability on Cavity in East Opencast Coal Mine. *Coal Proj.* **2018**, *50*, 10–13.
33. Aref, M.; Nei, L.; Abdo, S. Causes of rock falls in Ai-lluway-shaharea, Yemen. *Glob. Geol.* **2009**, *12*, 5–12.
34. Kawamoto, T.; Ichikawa, Y.; Kyoya, T. Deformation and fracture behaviour of discontinuous rock mass and damage mechanics theory. *Int. J. Numer. Anal. Methods Geomech.* **1988**, *12*, 1–30. [[CrossRef](#)]
35. Ju, Y.; Wang, Y.; Su, C.; Zhang, D.; Ren, Z. Numerical analysis of the dynamic evolution of mining-induced stresses and fractures in multilayered rock strata using continuum-based discrete element methods. *Int. J. Rock Mech. Min. Sci.* **2019**, *113*, 191–210. [[CrossRef](#)]
36. Gao, L.; Kang, X.T.; Huang, G.; Wang, Z.Y.; Tang, M.; Shen, X.Y. Experimental Study on Crack Extension Rules of Hydraulic Fracturing Based on Simulated Coal Seam Roof and Floor. *Geofluids* **2022**, 2022. [[CrossRef](#)]
37. Kong, D.; Xiong, Y.; Cheng, Z.; Wang, N.; Wu, G.; Liu, Y. Stability analysis of coal face based on coal face-support-roof system in steeply inclined coal seam. *Geomech. Eng.* **2021**, *25*, 233–243.
38. Donnelly, L.J.; Cruz, H.D.L.; Asmar, I.; Zapata, O.; Perez, J.D. The monitoring and prediction of mining subsidence in the Amaga, Angelopolis, Venecia and Bolombolo regions, Antioquia, Colombia. *Eng. Geol.* **2001**, *59*, 103–114. [[CrossRef](#)]